*chemistry*

MDPI

*Article*

# In Situ FBG Monitoring of a Henequen-Epoxy Biocomposite: From Manufacturing to Performance

**Mauricio Torres [1,*], Ana V. Rentería-Rodríguez [1] and Edgar A. Franco-Urquiza [2]**

[1] Center for Engineering and Industrial Development, Pie de la Cuesta 702, Queretaro 76125, Mexico; ana.renteria@cidesi.edu.mx
[2] CONACYT-National Center for Aeronautics Technologies, Carretera Estatal 200, Queretaro 76270, Mexico; edgar.franco@cidesi.edu.mx
* Correspondence: mauricio.torres@cidesi.edu.mx; Tel.: +52-442-2119800-5333

**Abstract:** This work reports the in situ instrumentation from manufacturing to loading of a henequen fiber woven-bioepoxy composite. Continuous monitoring was performed by means of fiber Bragg gratings (FBG) with the aim of tracking the curing behavior of the biolaminate by vacuum-assisted resin infusion (VARI). The instrumented composite was later tested mechanically under bending. Among the results obtained, micro-deformations were detected as a consequence of curing residual stresses, and when tested, the FBG data had similarity with the strain calculated according to the ASTM D7264/D7264M standard.

**Keywords:** henequen; bioepoxy; fiber Bragg gratings; VARI



**Citation:** Torres, M.; Rentería-Rodríguez, A.V.; Franco-Urquiza, E.A. In Situ FBG Monitoring of a Henequen-Epoxy Biocomposite: From Manufacturing to Performance. *Chemistry* **2022**, *4*, 380–392. https://doi.org/10.3390/chemistry4020028

Academic Editor: Pietro Russo

Received: 12 March 2022
Accepted: 24 April 2022
Published: 28 April 2022



## 1. Introduction

During the last decade, composite materials have increased significantly in the most critical sectors of the industry. Unlike metals or plastics, these materials have anisotropic properties, which means, in terms of mechanical and thermal performance, it is more difficult to predict their behavior under different physical or mechanical loads [1,2]. Owing to the complexity of their manufacture, whose process variables influence their final properties, determination of their initial state and final performance under specific in-service loads becomes challenging. However, with their increase in structural applications, there has been a strong call to understand their main characteristics and behavior using various techniques and methods to track these composites' performance during their life [3].

Natural fiber-reinforced polymer (NFRP) composites are of great interest due to their environmentally friendly nature [4]. Currently, research is focused on NFRP composed of vegetable fibers, such as sisal [5,6], kenaf [7], or jute [8–10], impregnated with bio-based resins such as epoxy vegetable oil (EVO) [11,12]. However, the degradation of natural components leads to structural failures that produce direct and indirect economic losses. Therefore, monitoring the structural integrity of these eco-friendly composites is crucial.

Structural health monitoring (SHM) is classified into active and passive monitoring. The first one generates predictive data from detection and action devices to warn of possible problems and promote preventive or corrective actions. The second one reveals a global perspective using actual performance data to provide information regarding composite integrity.

Integrated instrumentation used in biocomposites is a current approach with multiple applications. The sensors of these instruments provide relevant information about the integrity of the composite at any time, a technological challenge for many academies and industries worldwide [3,13]. Many techniques are capable of detecting damage or failure in structures. One of them, the bulk sensors used in composites, has been extensively studied [3,13–15]. These sensors are classified into (1) electrical and (2) optical devices. Electrical devices convert external stimuli into an electrical change in terms of current

or potential resistance. In this classification, we can find thermocouples [15], pressure transducers [16], piezoelectric sensors [17], and dielectric analysis devices (DEA) [18,19]. Optical devices take advantage of the disturbance of a light beam in terms of wavelength or period to quantify an external phenomenon. Fiber-optic devices can be classified into those that work according to Snell's law [20,21] and those that are based on the Bragg refractive index [22–26].

Currently, the most suitable sensors for the embedded instrumentation of composite structures are optical fibers with Bragg gratings (fiber Bragg gratings—FBG). For two decades, the investigation of this technology has demonstrated its added value in identifying physical parameters such as temperature changes and deformations inside composite structures during their fabrication under mechanical loads [13,22–26]. Among the advantages of these optical devices is their ease of integration into composite materials thanks to their fibrous shape and size (typically 250 µm), comparable to the thickness of a composite layer. Furthermore, they have a negligible impact on the mechanical behavior of the structure, immunity to electromagnetic fields, and a competitive production cost. However, Bragg gratings are very sensitive to temperature variations, so there is always a thermomechanical coupling in the measurements acquired, which implies separating thermal and mechanical information; this is a laborious task and demands sensitivity to the fiber optics used [13,23,24]. In addition, this technique commonly requires a cable link to transmit the data, which requires adapting the connections, especially during the part-manufacturing phase [13,23,24]. Despite its multiple benefits, FBG technology has not been widely applied in biocomposites, and this is the gap that this research aims to cover.

Fiber Bragg gratings are the fundamental elements upon which most fiber optic sensors are based. An FBG is a reflector inside the core of the fiber that is set to a specific wavelength of light. These reflective micro-surfaces modify the wavelength of the Bragg reflection peak ($\Delta\lambda_B$) of the transmitted light wave, which depends on the grating distance. Light travels along the fiber axis in a single optical fiber, keeping a constant wavelength ($\lambda_{B0}$) as long as the same spacing between the gratings is maintained. Deformation is given by the variation in the gratings' separation and modifying the wavelength that passes through them (Equation (1)).

$$K\varepsilon = \frac{\Delta L}{L} = \frac{\Delta\lambda_B}{\lambda_{B0}} \tag{1}$$

Any change in the axial/transverse strain ($\Delta\varepsilon_B$) or the temperature ($\Delta T$) of the fiber induces a variation in the grating period or the refractive index. The measurable result is a change in the Bragg peak, which indicates external stimuli (Equation (2)).

$$\Delta\lambda_B = \lambda_{B0}(1 - p_e)\Delta\varepsilon_B + \lambda_{B0}(\alpha_e + \xi_B)\Delta T \tag{2}$$

where $p_e$ is the optical strain coefficient, $\alpha_e$ is the fiber's coefficient of thermal expansion (CTE), and $\xi_B$ is the fiber's thermo-optical coefficient.

FBGs can have a silica ($SiO_2$) or polymer basis. Recently, polymer optical fiber Bragg gratings (POFBGs) have received more attention because of their sensing capabilities compared with their silica equivalents. Other features are their flexibility and biocompatibility, which can expand their application on biomaterials [27,28].

Because of the operating principle and the capabilities of the FBG, it has been considered a convenient device to monitor materials whose application requires constant vigilance, anticipating possible failures due to deformation or fatigue. In this way, the goal of this work is to carry out FBG monitoring to record in situ the manufacturing processes and mechanical testing of biocomposites. The first appearance of the strains is related to the thermal variations during the configuration of infusion, resin infusion, gelation, curing, and release. In this way, knowing the first deformations of the biocomposite, we will be able to estimate its influence on the resulting mechanical properties and follow its behavior until the end of the useful life of these eco-friendly materials.

## 2. Materials and Methods

### *2.1. Henequen Fiber*

The henequen fiber used belongs to the Asparagus family, spun in the Cordelería Santa Inés, Yucatán, Mexico, with strands of 30 to 35 threads. The average length of the strand is 2000 m. Subsequently, the strand was manufactured on a manual loom by Mexican textile artisans from Querétaro, with a flat biaxial-weaving configuration. The mechanical properties of the henequen yarn are cited in [10], according to the ASTM C1557 and D3822 standards. According to these standards, henequen fibers have 13.21 $\pm$ 2.45 MPa of tensile strength, 12.92 $\pm$ 4.12 GPa of elastic modulus, and a density of 1.12 $\pm$ 0.01 g/c (Torres et al. [10]).

### *2.2. Biobased Resin*

Epoxy resin Surf Clear from Sicomin Epoxy Systems (Sicomin, Châteauneuf les Martigues, France), with a resin-hardener ratio of 100:41, was used. The resin is an epoxidized vegetable oil (EVO) with a biobased carbon content of 49%. Based on the information from the manufacturer, the chemical structure of the resin does not contain agents that are harmful to the environment due to its low viscosity, compatibility with synthetic fibers, and good biodegradability, being an alternative for laminates made by infusion. Regarding its mechanical behavior, it is reported to have an elastic modulus of 3.4 GPa, a tensile strength of 68 MPa, and an elongation of 6.5% (Torres et al. [10]).

### *2.3. FBG Sensor and Interrogator*

The Micron Optics® (Atlanta, GA, USA) os1100 FBG is a sensor used to monitor temperature and stress and is available in several different wavelengths. It is a single FBG centered in a two-meter length of polyimide-coated optical fiber.

The optical-fiber type is SMF28 compatible with a length of 10 mm, coated-fiber diameter of 145–165 mm, a wavelength of 1560 nm, strain range of $-5000$ to +5000 $\mu\varepsilon$, mechanical sensitivity of $\approx$1.2 pm/$\mu\varepsilon$, temperature range of $-40$ °C to 120 °C, and thermal sensitivity of $\approx$9.9 pm/°C. These characteristics facilitate the FBG integration inside composite materials to monitor the manufacturing and testing process. It is used in basic applications and for the construction of complex transducers containing one or more FBGs. It has a polyimide coating that provides good stress transfer through the fiber and performs well over a wide temperature range.

Micron Optics® (Atlanta, GA, USA) si155 Standard 1400 interrogator was used for experimentation. The fiber-optic interrogator is an optical signal processing instrument that sends a light signal in a specific frequency band to the fiber optic sensors, which reflect part of the signal back to the interrogator, carrying information regarding strain and temperature to which they are subjected. The fiber-optic interrogator includes ENLIGHT® (Atlanta, GA, USA) software that allows optical signal processing and real-time tracking and monitoring of the instrumented structure.

### *2.4. Vacuum Assited Resin Infusion Process (VARI)*

Vacuum-assisted infusion resin (VARI) is the most common composite fabrication procedure because of its simplicity, low cost, and flexibility when experimenting with new fibers and resins. The VARI setup consisted of placing two biaxial plies of henequen fiber with a flat fabric of 200 GSM with dimensions of 40 cm $\times$ 60 cm. An optical fiber was placed between the two fiber sheets, which served as a monitor during the entire manufacturing and testing process. The setup and manufacturing procedure are described in detail below.

First, release wax is placed in a rectangular glass mold. Next, the first henequen preform is placed. Then, the optic-fiber sensor with Bragg grating is placed and fixed at the ply's ends with adhesive tape. At this time, the optical fiber is interrogated while the second sheet of the henequen preform is placed. At this time, a compaction roller is passed to exert a distributed load along the optical fiber. Subsequently, infusion supplies are placed: (i) resin flow line, (ii) peel-ply, (iii) resin flow media, (iv) sealant tape, and (v) vacuum bag

were placed, as depicted in Figure 1. After that, when sealing the bag, a compaction is made with the roller on the position of the optical fiber to simulate an instantaneous point load.

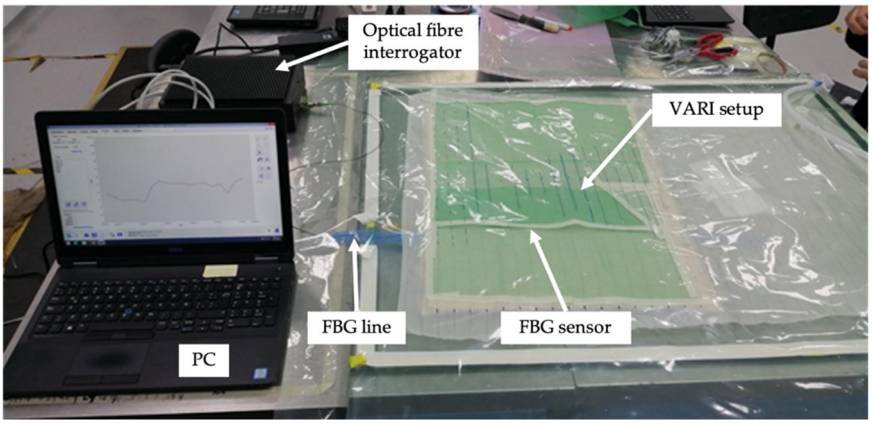


**Figure 1.** VARI setup for monitoring biocomposite fabrication with FBG optical fiber.

Once the henequen preform and the supplies have been placed, compaction vacuum is applied. This is done to (i) verify the tightness of the bag, (ii) identify air leak points on the seal tape, (iii) verify that the pressure is uniform, and (iv) avoid sharp points that could shred bag. Subsequently, the vacuum bag is sealed by closing the resin inlet and outlet. When resin inlet is open, infusion starts, tracking the path of the flow resin and interrogating the FBG in the meantime. For the infusion process, the vacuum is −21 inHg, and the curing temperature is 25 °C. Curing is tracked by the FBG as well as the composite demolding. Finally, the ply thickness of the FBG instrumented biocomposite is 1.5 mm, with a fiver volume fraction of 24.9% and resin volume fraction of 75.1% (Figure 2).

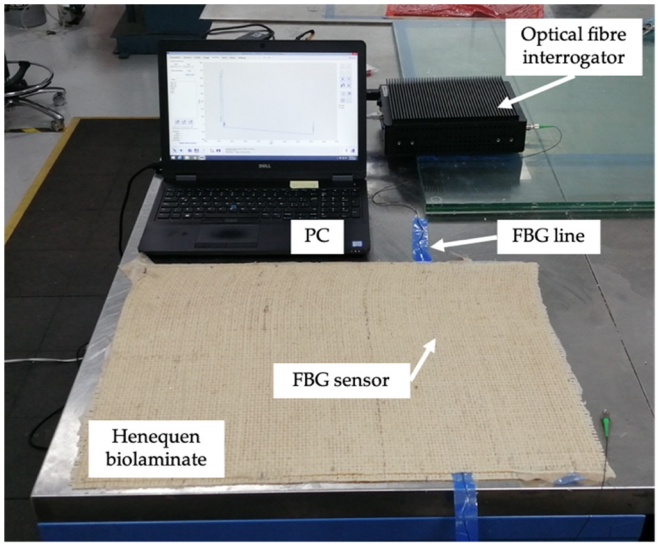


**Figure 2.** Instrumented biocomposite with FBG optical fiber.

### *2.5. Mechanical Characterization by Bending*

Three-point bending tests, based on the ASTM D7264 standard, were performed on an Instron 647 (Norwood, MA, USA) universal testing machine with a load cell of 1 kN. FBG-instrumented biolaminate coupons have 400 × 50 × 3 mm as nominal dimensions (Figure 3a). Span was set at 120 mm, and crosshead speed was 1.27 mm/min (equivalent to 0.5 in/min). During the bending test, 5 load cycles with durations of 1 min, 2 min, 3 min, 4 min, and 5 min were carried out in order to observe the evolution of the micro-strains inside the material by increasing the amount of load.

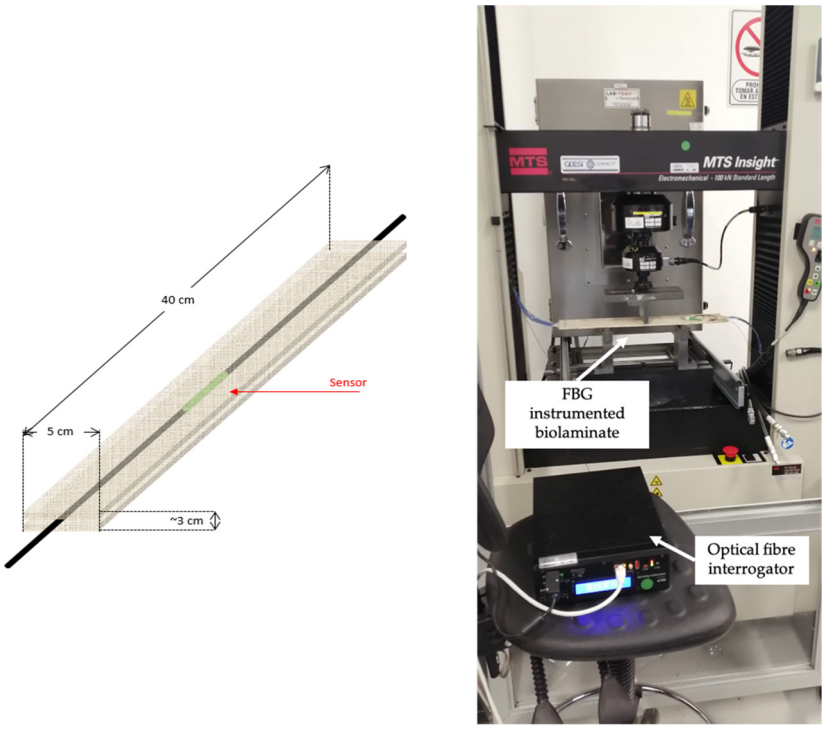


(**a**) (**b**)

**Figure 3.** (**a**) FBG biolaminate coupon, (**b**) three-point bending test configuration.

## 3. Results

### *3.1. VARI Tracking for a FBG Instrumented Biocomposite*

As described in the previous section, the continuous monitoring of the fabrication process of a henequen-epoxy biolaminate is performed by means of an FBG optical fiber sensor. First, at the fabric setup, it is identified that the weight of the henequen preforms and the VARI supplies create a deformation of approximately 50 microstrains (με), as shown in Figure 4.

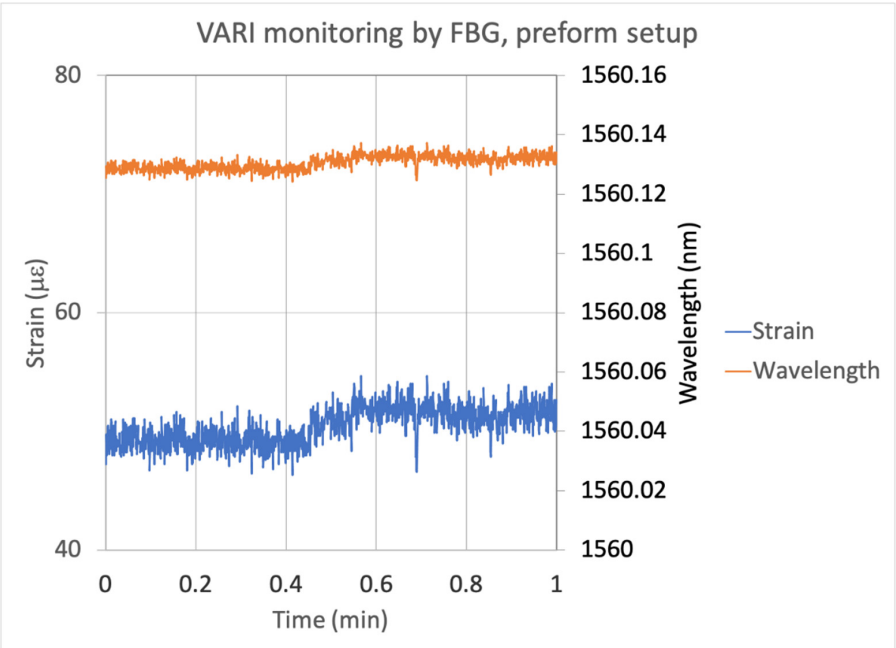


**Figure 4.** VARI monitoring by FBG, preform setup.

Then, when sealing the bag, we can identify the instantaneous point load caused by the compaction roller, producing a deformation of 130 με. Figure 5 shows the response of the sensor at this stage.

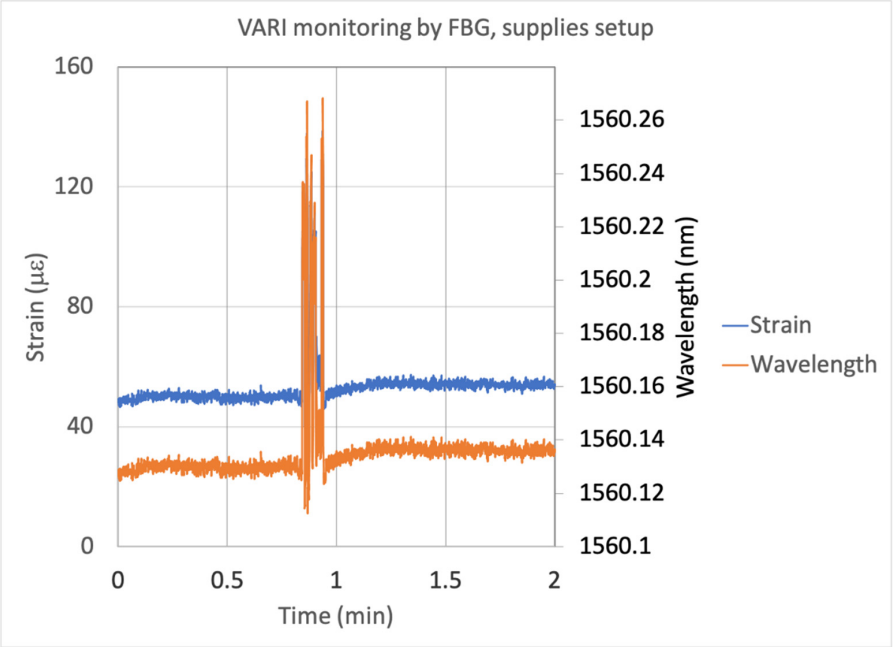


**Figure 5.** VARI monitoring by FBG, supplies setup with point loads to verify sensor sensitivity.

Atmospheric pressure at this height causes the strain to be approximately 700 με when continuous vacuuming is applied. In addition, two increases in deformation are identified, 1000 με and 850 με, due to exert point loads with the compaction roller, as shown in Figure 6. When the vacuum bag is sealed by closing the resin inlet and outlet, the vacuum pressure triggers a maximum strain of 600 με, as illustrated in Figure 7.

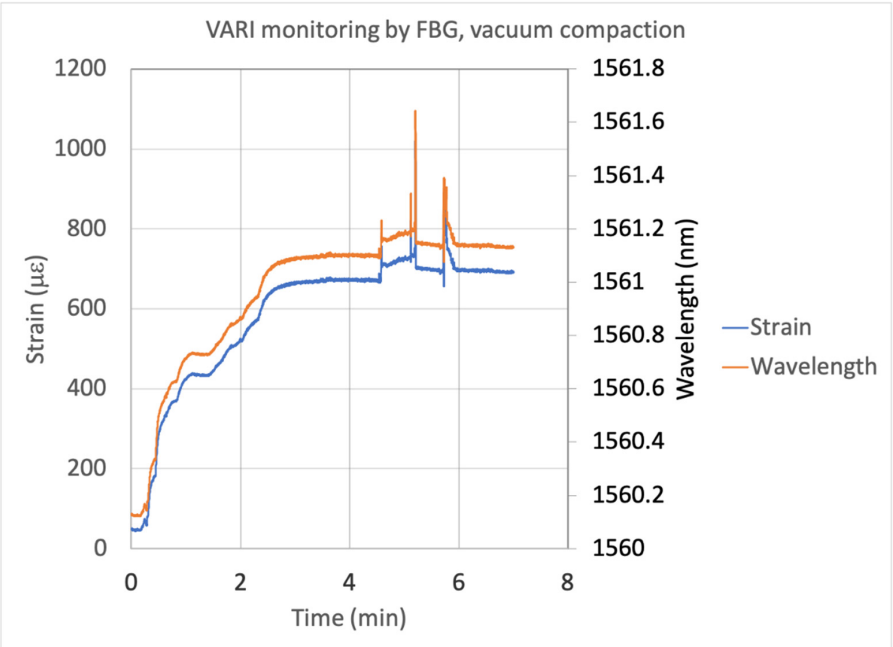


**Figure 6.** VARI monitoring by FBG, vacuum compaction with point loads at FBG location.

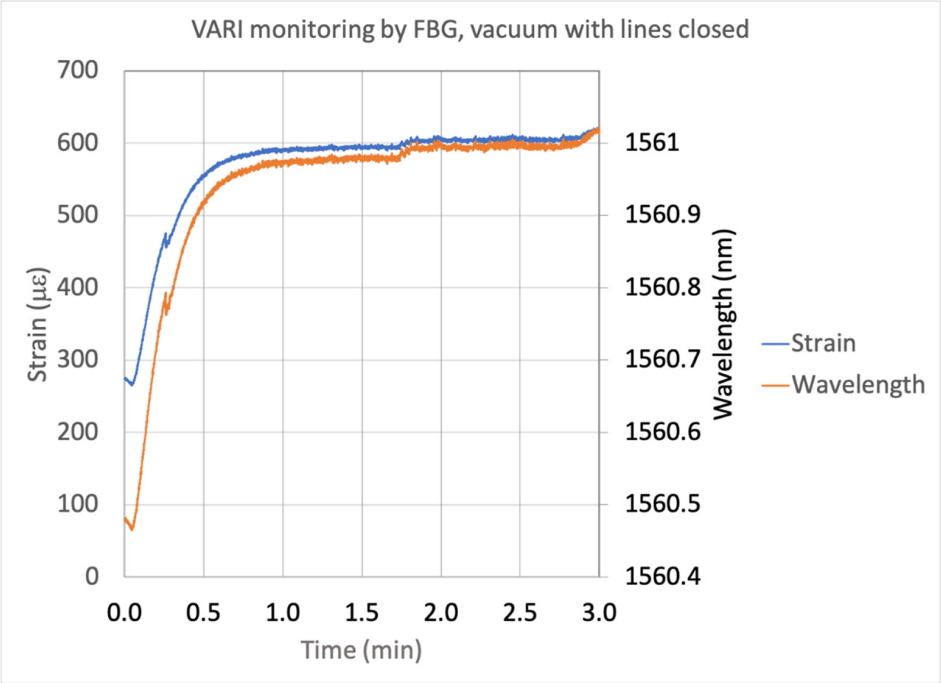


**Figure 7.** VARI monitoring by FBG, vacuum with air-resin lines closed, ready for infusion.

By the time resin infusion begins, the FBG captures a drop on the internal strains. Attenuation of the strains is observed 10 min after the resin inlet is open, with a value of 100 με, reaching −50 με at the lowest strain value, which is illustrated in Figure 8.

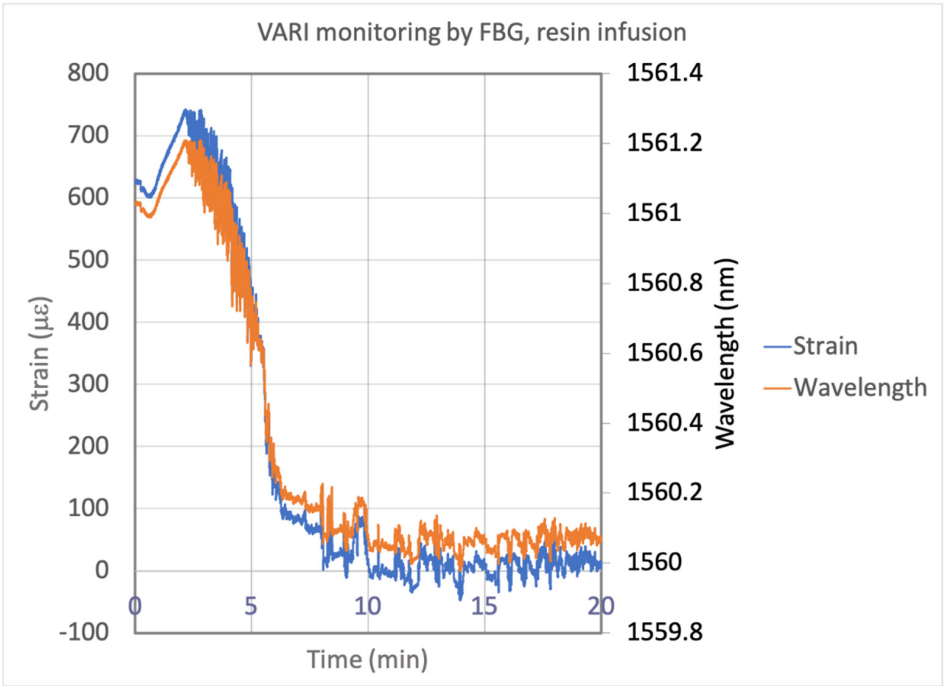


**Figure 8.** VARI monitoring by FBG, resin infusion, measuring the evolution of the flow front.

When curing starts, there is a more notable variation in the microstrains sensed by the FBG, as shown in Figure 9. Curing strain initial value is −50 με and reaches an average value of 25 με after 1 h. This is caused by the exothermic reaction, which contributes to the rising of inner microstrains.

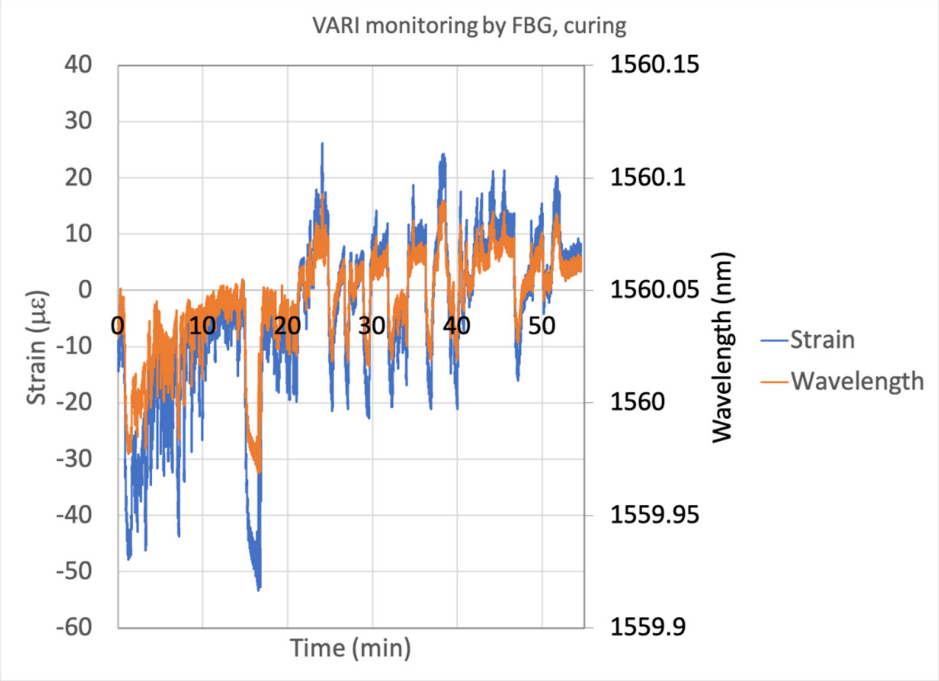


**Figure 9.** VARI monitoring by FBG, composite curing, identifying the first residual strains.

When the composite is consolidated, a minor variation of microdeformations is noticed. These small variations (from −7 με to −20 με) are related to the solidification of the epoxy resin, forming the composite's microstructure, as shown in Figure 10.

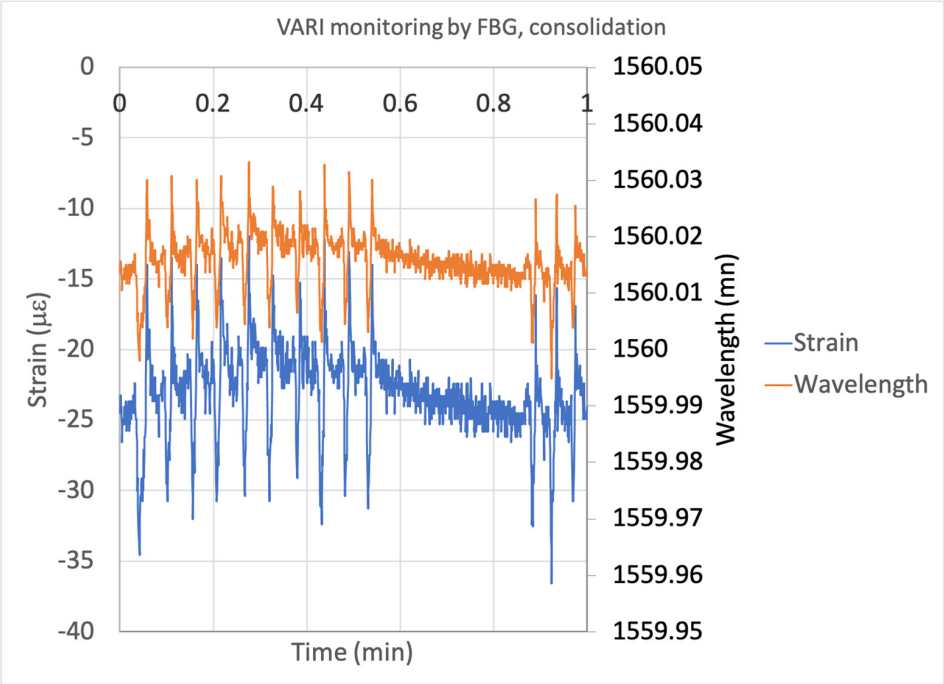


**Figure 10.** VARI monitoring by FBG, composite consolidation, identifying the evolution of residual strains.

Prior to composite demolding, the residual strains reach −130 με. At the instant of demolding, a deformation peak is observed, −140 με, attributed to (i) the detachment from the mold and (ii) the temperature of the mold, which is near 50 °C. When the composite

is released, a spring-back effect is observed, and the value of residual strains returns to −105 με, as depicted in Figure 11.

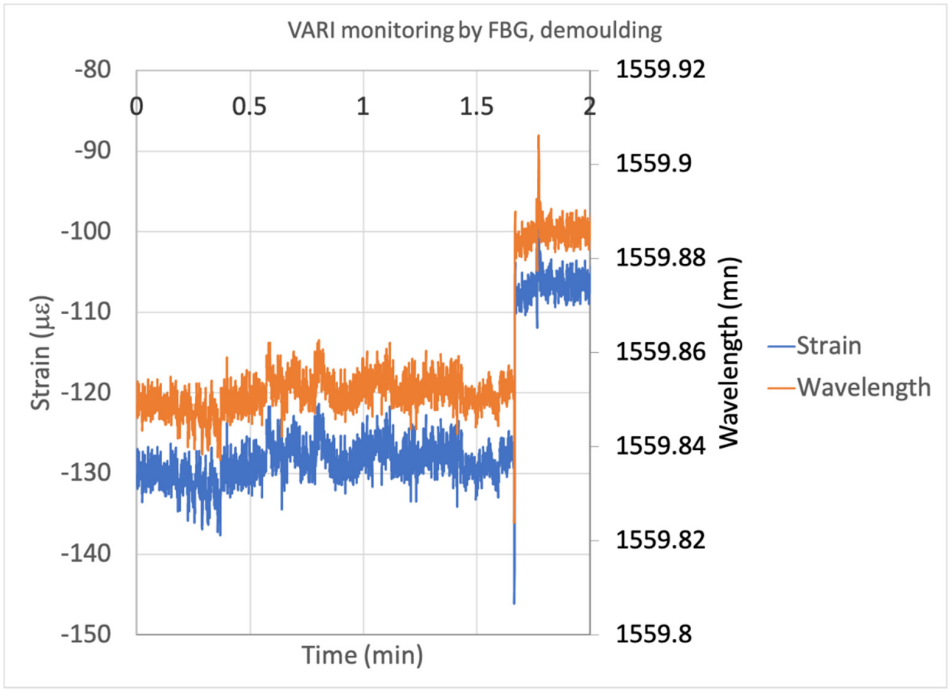


**Figure 11.** VARI monitoring by FBG, composite demolding with spring-back effect.

Finally, the composite plate cools off at room temperature (RT = 25 °C). The residual strains at this point appear between −50 με and −60 με. To verify the sensitivity of the FBG to external mechanical stimuli, the compaction roller is passed over the location of the optical fiber sensor, giving measurements below −70 με, as illustrated on Figure 12.

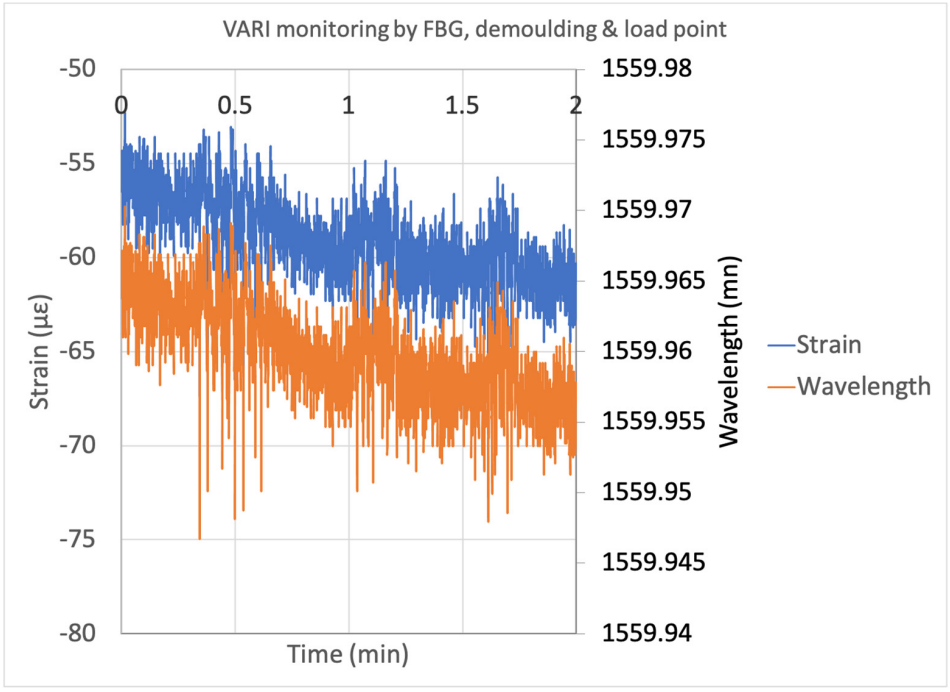


**Figure 12.** VARI monitoring by FBG, composite at room temperature with pressure loads.

### *3.2. Mechanical Characterization Tracking for a FBG Instrumented Biocomposite*

Continuous monitoring for the mechanical behavior of a henequen-epoxy biolaminate is performed by means of a FBG optical fiber sensor. For the calculation of the stress under bending, the ASTM D7264M—15 standard is considered in which the following equation is presented:

$$\sigma = \frac{3PL}{2bh^2} \tag{3}$$

where $\sigma$ is the outer surface stress in the load span region (MPa), $P$ is the applied load (N), $L$ is the support span (mm), $b$ is the width of the specimen (mm), and $h$ is the thickness of the specimen (mm). Meanwhile, to calculate the deformations, the following equation is used:

$$\varepsilon = \frac{6\delta h}{L^2} \tag{4}$$

where $\varepsilon$ is the maximum strain on the outer surface (mm/mm), $\delta$ is the mid-span deflection (mm), $L$ is the span support (mm), and $h$ is the thickness of the specimen (mm).

The objective of observing the loading and unloading behavior of the instrumented biolaminate has two purposes: the first one is to corroborate the well-functioning behavior of the FBG during the test, whereas the second one is to know the evolution of the inner microstrains of the biolaminate throughout the in-service load.

The data obtained from the strains recorded by the FBG were plotted in comparison with the strains calculated from the ASTM standard, which results from the relationship between the deflection, the thickness, and the span of the composite. As depicted in Figure 13, the strain measurements obtained by the FBG and the strain values calculated from the mechanical standard show a similar linear trend for each load repetition.

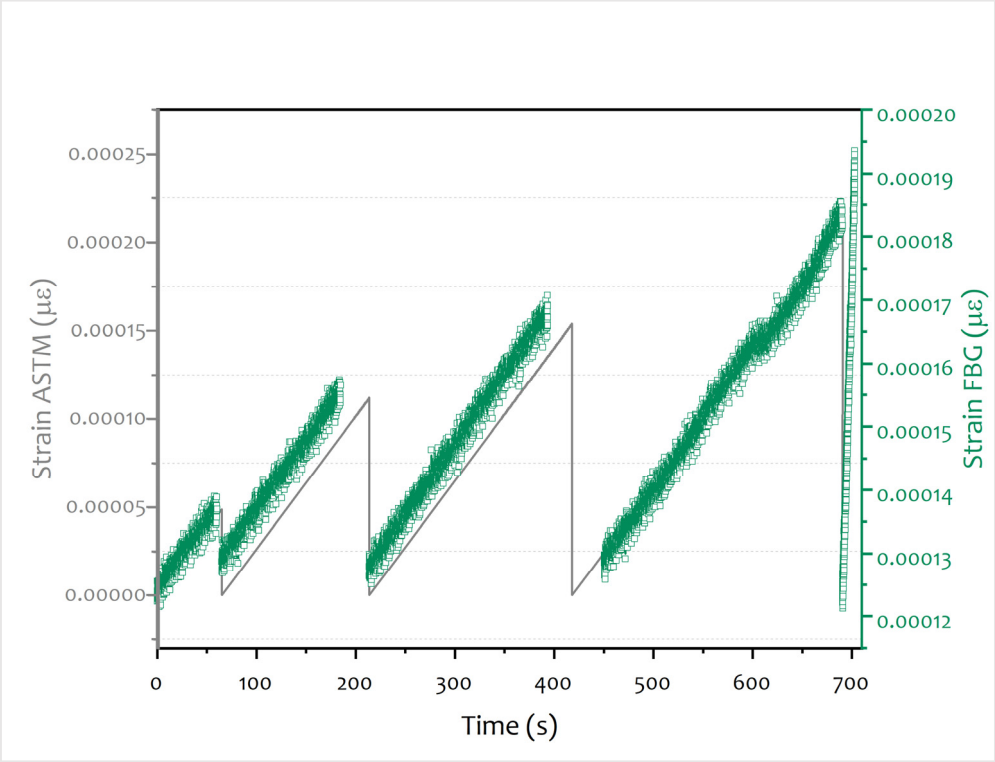


**Figure 13.** Load-unload cycles for the FBG instrumented henequen biolaminate, showing the evolution of strain by calculation (gray line) and FBG measurements (green dots).

## 4. Discussion

By using an in-core FBG optical fiber sensor to track the whole fabrication procedure of a biolaminate composite, some highlights can be announced.

First, at preform setup, the weight of the henequen fabrics and the VARI supplies create a uniform deformation value of 50 με. As all supplies act as a distributed load on the optic fiber sensor, sudden peaks of deformation are not shown.

Second, when vacuum is applied, the strain raises till 650 με and then drops because the inlet-outlet lines are clamped. Then a deformation peak of 750 με occurs as a result of the vacuum pump resuming air suction. Subsequently, there is a decline in the deformations, a result of the impregnation of the preform with the resin. At this stage, the FBG optical fiber sensor is surrounded by resin, representing a solid immersed in a liquid, causing the atmospheric pressure load to drop.

Third, at the composite's gelation and curing, there is a decrease in the inner strains, which is a characteristic of a contraction in the thermoset resin. The change of the polymer's density is related to the amount of cross-linking [29,30]. The formation of the microstructure of the material affects the space of the FBG grids. Moreover, as curing causes an exothermic reaction, the coupled strains due to the temperature changes are also captured.

Fourth and finally, at the demolding stage, deformation peaks are observed due to the spring-back effect. This phenomenon is related to the difference in the coefficient of thermal expansion (CTE) between the biocomposite and the metal mold.

As can be noticed, an average of −50 με is recorded as the initial strain state for a henequen biocomposite, and is not negligeable for mechanical purposes.

For the biolaminate mechanical performance, as the load cycles go by, the initial deformations in each cycle increase, following a linear behavior. It is highlighted that initial FBG deformation value corresponds to the value recorded from the demolding stage. For the deformation calculated by the standard, the strain value is zero because no deflection of the composite beam is provided. When the load is applied, the inner strains must be calculated at the FBG location, considering its proximity to the middle thickness of the biolaminate. As illustrated in Figure 14, the strains calculated show a gradual increment due to the deflection of the beam, whereas the FBG strains show a change in sign and evolve linearly. Both strain estimation methods are congruent and confirm, first, the in situ detection of mechanical phenomena by FBG, and second, the presence of residual strains after manufacturing and curing.

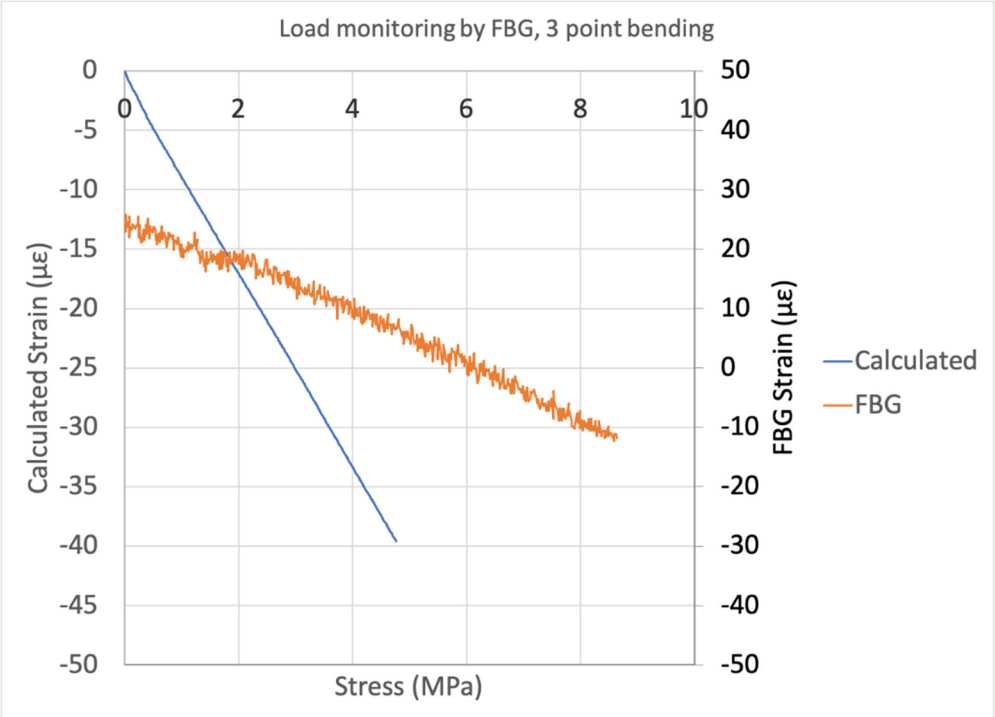


**Figure 14.** Comparison between FBG and ASTM calculated strains for the 1 min load cycle.

## 5. Conclusions

A henequen fiber/EVO resin composite material was manufactured by vacuum-assisted resin infusion and in-core instrumented with an FBG optical fiber sensor.

The FBG was incorporated to monitor the entire manufacturing process as well as the mechanical tests.

The strains resulting from all manufacturing steps, which included (i) preform setup, (ii) supplies placing, (iii) vacuum, (iv) resin infusion, (v) curing and (vi) demolding, were recorded. The composite setup results were an average of 50 $\mu\varepsilon$, and when vacuuming was applied, strains reached 700 $\mu\varepsilon$. Curing caused a change in compression strains, with an average of $-130$ $\mu\varepsilon$. Finally, composite demolding set the residual strains at $-75$ $\mu\varepsilon$.

For the mechanical tests, it was shown that the deformations can be faithfully monitored by the FBG in comparison with those standardized. Therefore, the measurement of the deformations by the FBG are reliable and comparable with other structural health-monitoring methods.

Further work can be focused on detecting interlaminar failures based on the deformations recorded by the FBG, despite the fact that no superficial damage was observed.

## 6. Patents

There are no patents resulting from the work reported in this manuscript.

**Author Contributions:** Conceptualization, M.T.; methodology, M.T.; formal analysis, M.T. and A.V.R.-R.; investigation, A.V.R.-R.; resources, E.A.F.-U.; data curation, A.V.R.-R.; writing—original draft preparation, M.T.; writing—review and editing, A.V.R.-R. and E.A.F.-U.; supervision, E.A.F.-U.; project administration, E.A.F.-U.; funding acquisition, E.A.F.-U. All authors have read and agreed to the published version of the manuscript.

**Funding:** This research was funded by CONACYT, grant number 257458 & 275783, and the APC was funded by CONACYT, grant number 257458.

**Institutional Review Board Statement:** Not applicable. These studies do not involve humans or animals.

**Informed Consent Statement:** Not applicable. These studies do not involve humans.

**Data Availability Statement:** This study did not report any data.

**Acknowledgments:** Authors thank the participation of M. Sc. Victor Gómez Culebro for the VARI setup and Technician Sergio López for the coupon preparation.

**Conflicts of Interest:** The authors declare no conflict of interest. The funders had no role in the design of the study; in the collection, analyses, or interpretation of data; in the writing of the manuscript, or in the decision to publish the results.

## References

1. Thyavihalli-Girijappa, Y.G.; Rangappa, S.M.; Parameswaranpillai, J.; Siengchin, S. Natural fibers as sustainable and renewable resource for development of eco-friendly composites: A comprehensive review. *Front. Mater.* **2019**, *6*, 226–240. [CrossRef]
2. Ramesh, M.; Palanikumar, K.; Reddy, K.H. Comparative Evaluation on Properties of Hybrid Glass Fiber-Sisal/Jute Reinforced Epoxy Composites. *Procedia Eng.* **2013**, *51*, 745–750. [CrossRef]
3. Torres, M. Parameters' monitoring and in-situ instrumentation for resin transfer moulding: A review. *Compos. Part A Appl. Sci. Manuf.* **2019**, *124*, 105500. [CrossRef]
4. Parbin, S.; Waghmare, N.K.; Singh, S.K.; Khan, S. Mechanical properties of natural fiber reinforced epoxy composites: A review. *Procedia Comput. Sci.* **2019**, *152*, 375–379. [CrossRef]
5. Torres, M.; Rentería, A.V.; Alcántara, P.I.; Franco-Urquiza, E. Mechanical properties and fracture behaviour of agave fibers bio-based epoxy laminates reinforced with zinc oxide. *J. Ind. Text.* **2020**, 1–22. [CrossRef]
6. Binoj, J.S.; Bibin, J.S. Failure analysis of discarded agave tequilana fiber polymer composites. *Eng. Fail. Anal.* **2019**, *95*, 379–391. [CrossRef]
7. Santulli, C.; Sarasini, F.; Tirillo, J.; Valente, T.; Valente, M.; Caruso, A.P.; Infantino, M.; Nisini, E.; Minak, G. Mechanical behaviour of jute cloth/wool felts hybrid laminates. *Mater. Des.* **2013**, *50*, 309–321. [CrossRef]
8. Salman, S.D. Effects of jute fibre content on the mechanical and dynamic mechanical properties of the composites in structural applications. *Def. Technol.* **2020**, *16*, 1098–1106. [CrossRef]

9. Mahesh, V.; Joladarashi, S.; Kulkarni, S.M. Influence of laminate thickness and impactor shape on low velocity impact response of jute-epoxy composite: FE study. *Mater. Today Proc.* **2020**, *28*, 545–550. [CrossRef]
10. Torres, M.; Rentería, A.V.; Franco-Urquiza, E. Mechanical properties of natural-fiber-reinforced biobased epoxy resins manufactured by resin infusion process. *Polymers* **2020**, *12*, 2841. [CrossRef] [PubMed]
11. Kuo, P.Y.; Sain, M.; Yan, N. Synthesis and characterization of an extractive-based bio-epoxy resin from beetle infested Pinus contorta bark. *Green Chem.* **2014**, *16*, 3483–3493. [CrossRef]
12. Ozer, E.; Feng, M.Q. *Start-Up Creation*; Woodhead Publishing Series in Civil and Structural Engineering; Woodhead Publishing: Thorston, UK, 2020; pp. 345–367.
13. Collombet, F.; Torres, M.; Douchin, B.; Crouzeix, L.; Grunevald, Y.H.; Lubin, J.; Camps, T.; Jacob, X.; Luyckx, G.; Wu, K.T. Multi-instrumentation monitoring for the curing process of a composite structure. *Measurement* **2020**, *157*, 107635. [CrossRef]
14. Matsuzaki, R.; Kobayashi, S.; Todoroki, A.; Mizutani, Y. Cross-sectional monitoring of resin impregnation using an area-sensor array in an RTM process. *Compos. Part A Appl. Sci. Manuf.* **2012**, *43*, 695–702. [CrossRef]
15. Yenilmez, B.; Sozer, E.M. A grid of dielectric sensors to monitor mold filling and resin cure in resin transfer molding. *Compos. Part A Appl. Sci. Manuf.* **2009**, *40*, 476–489. [CrossRef]
16. Tuncol, G.; Danisman, M.; Kaynar, A.; Sozer, E.M. Constraints on monitoring resin flow in the resin transfer molding (RTM) process by using thermocouple sensors. *Compos. Part A Appl. Sci. Manuf.* **2007**, *38*, 1363–1386. [CrossRef]
17. Di Fratta, C.; Klunker, F.; Ermanni, P. A methodology for flow-front estimation in LCM processes based on pressure sensor. *Compos. Part A Appl. Sci. Manuf.* **2013**, *47*, 1–11. [CrossRef]
18. Kobayashi, M.; Jen, C.K. Piezoelectric thick bismuth titanate/PZT composite film transducers for smart NDE of metals. *Smart Mater. Struct.* **2004**, *13*, 951–956. [CrossRef]
19. Boll, D.; Schubert, K.; Brauner, C.; Lang, W. Miniaturized flexible interdigital sensor for In situ dielectric cure monitoring of composite materials. *IEEE Sens. J.* **2014**, *14*, 2193–2197. [CrossRef]
20. Lekakou, C.; Cooka, S.; Denga, Y.; Angb, T.W.; Reed, G.T. Optical fibre sensor for monitoring flow and resin curing in composites manufacturing. *Compos. Part A Appl. Sci. Manuf.* **2006**, *37*, 934–938. [CrossRef]
21. Grande, A.M.; Di Landro, L.; Bettini, P.; Baldi, A.; Sala, G. RTM process monitoring and strain acquisition by fibre optics. *Proc. Eng.* **2011**, *10*, 3497–3502. [CrossRef]
22. Baker, W.; McKenzie, I.; Jones, R. Development of life extension strategies for Australian military aircrafts using structural health monitoring of composite repair joints. *Compos Struct* **2004**, *66*, 133–143. [CrossRef]
23. Hernández, H.; Collombet, F.; Douchin, B.; Choqueuse, D.; Davies, P.; González, J.L. Entire life-time monitoring of filament wound composite cylinders using Bragg grating sensors: I. Adapted tooling and instrumented specimen. *Appl. Compos. Mater.* **2009**, *16*, 173–182. [CrossRef]
24. Hernández, H.; Collombet, F.; Douchin, B.; Choqueuse, D.; Davies, P.; González, J.L. Entire life-time monitoring of filament wound composite cylinders using Bragg grating sensors: II. Process Monitoring. *Appl. Compos. Mater.* **2009**, *16*, 197–209. [CrossRef]
25. Hernández, H.; Collombet, F.; Douchin, B.; Choqueuse, D.; Davies, P.; González, J.L. Entire life-time monitoring of filament wound composite cylinders using Bragg grating sensors: III. In-service external pressure loading. *Appl. Compos. Mater.* **2009**, *16*, 135–147. [CrossRef]
26. Khoun, L.; de Oliveira, R.D.; Michaud, V.; Hubert, P. Investigation of process-induced strains development by fibre Bragg grating sensors in resin transfer moulded composites. *Compos. Part A Appl. Sci. Manuf.* **2011**, *42*, 274–282. [CrossRef]
27. Pospori, A.; Marques, C.A.F.; Bang, O.; Webb, D.J.; André, P. Polymer optical fiber Bragg grating inscription with a single UV laser pulse. *Opt. Express* **2017**, *25*, 9028–9038. [CrossRef] [PubMed]
28. Marques, C.A.F.; Min, R.; Leal-Junior, A.; Antunes, P.; Fasano, A.; Woyessa, G.; Nielsen, K.; Rasmussen, H.K.; Ortega, B.; Bang, O. Fast and stable gratings inscription in POFs made of different materials with pulsed 248 nm KrF laser. *Opt. Express* **2018**, *6*, 2013–2022. [CrossRef] [PubMed]
29. Lascano, D.; Quiles-Carrillo, L.; Torres-Giner, S.; Boronat, T.; Montanes, N. Optimization of the curing and post-curing conditions for the manufacturing of partially bio-based epoxy resins with improved toughness. *Polymers* **2019**, *11*, 1354. [CrossRef]
30. Moller, J.C.; Berry, R.J.; Foster, H.A. On the nature of epoxy resin post-curing. *Polymers* **2020**, *12*, 466. [CrossRef]